

# Metabolomic profiling of a neurodegenerative retina following optic nerve transection

JUN-YA ZHU<sup>1,2\*</sup>, XI-SEN NI<sup>1,3\*</sup>, XIAO-YAN HAN<sup>2\*</sup>, SHA LIU<sup>1,3</sup>, YU-KE JI<sup>1,3</sup>, JIN YAO<sup>1,3</sup> and BIAO YAN<sup>2,4,5</sup>

<sup>1</sup>Department of Ophthalmology and Optometry, The Fourth School of Clinical Medicine, Nanjing Medical University, Nanjing, Jiangsu 210029; <sup>2</sup>Eye Institute and Department of Ophthalmology, Eye and Ear, Nose and Throat Hospital, State Key Laboratory of Medical Neurobiology, Fudan University, Shanghai 200030; <sup>3</sup>Department of Ophthalmology and Optometry, The Affiliated Eye Hospital, Nanjing Medical University, Nanjing, Jiangsu 210029; <sup>4</sup>National Health Commission Key Laboratory of Myopia, Chinese Academy of Medical Sciences; <sup>5</sup>Shanghai Key Laboratory of Visual Impairment and Restoration, Fudan University, Shanghai 200030, P.R. China

Received January 10, 2023; Accepted July 19, 2023

DOI: 10.3892/mmr.2023.13065

**Abstract.** The degeneration of retinal ganglion cells (RGCs) often causes irreversible vision impairment. Prevention of RGC degeneration can prevent or delay the deterioration of visual function. The present study aimed to investigate retinal metabolic profiles following optic nerve transection (ONT) injury and identify the potential metabolic targets for the prevention of RGC degeneration. Retinal samples were dissected from ONT group and non-ONT group. The untargeted metabolomics were carried out using liquid chromatography-tandem mass spectrometry. The involved pathways and biomarkers were analyzed using Kyoto Encyclopedia of Genes and Genomes (KEGG) pathway analysis and MetaboAnalyst 5.0. In the ONT group, 689 disparate metabolites were detected, including lipids and lipid-like molecules. A total of 122 metabolites were successfully annotated and enriched in 50 KEGG pathways. Among them, 'sphingolipid metabolism' and 'primary bile acid biosynthesis' were identified involved in RGC degeneration. A total of five metabolites were selected as the candidate biomarkers for detecting RGC degeneration with an AUC value of 1. The present study revealed that lipid-related metabolism was involved in the pathogenesis of retinal neurodegeneration.

Taurine, taurochenodesoxycholic acid, taurocholic acid (TCA), sphingosine, and galabiosylceramide are shown as the promising biomarkers for the diagnosis of RGC degeneration.

## Introduction

Retinal ganglion cells (RGCs) are the only neurons that transmit the visual information from the eye to brain retino-recipient areas via the optic nerves (1). The bodies of RGCs reside in the inner retina, while the long axons are located in retinal nerve fiber layer, forming the optic nerve head (2). Several pathological factors can cause RGC degeneration, such as compression and transection of optic nerve, retinal ischemia, intracranial hypertension, as well as photic and thermal damage (3). The degeneration of RGCs can lead to several irreversible blindness, including glaucoma (4), traumatic optic neuropathy (5) and optic neuritis (6). The mechanisms causing RGC degeneration include neurotrophic factor deprivation, axonal transport failure, mitochondrial dysfunction, excitotoxic damage, activation of apoptotic signals, oxidative stress, misbehaving reactive glia and loss of synaptic connectivity (7). In addition, RGC degeneration is associated with abnormal proteostasis, including dysregulation of protein translation, chaperone-assisted protein folding and protein degradation (8,9). Protein imbalance can lead to the activation of inflammatory pathways, excitotoxic lesions and oxidative stress. A variety of neuroprotective methods have been developed to reduce RGC degeneration, such as neurotrophic agents, steroid hormones, glutamate receptor antagonists, anti-oxidants and electrical stimulation (10). However, similar to other parts of central nervous system (CNS) in adult mammals, the degeneration of RGCs and axonal nerve fibers are difficult to regenerate (11). Currently, it is still a great challenge for restoring RGC function following RGC degeneration. Further study is still required to clarify the potential mechanism of RGC degeneration.

The optic nerve transection (ONT) model has been widely used to study the regeneration of RGCs and axonal regeneration (12). Approximately 80% of RGCs die within 2 weeks following RGC axon injury (13). A number of biomarkers have

*Correspondence to:* Dr Biao Yan, Eye Institute and Department of Ophthalmology, Eye and Ear, Nose and Throat Hospital, State Key Laboratory of Medical Neurobiology, Fudan University, 83 Fen Yang Road, Shanghai 200030, P.R. China  
E-mail: biao.yan@fdeent.org

Dr Jin Yao, Department of Ophthalmology and Optometry, The Fourth School of Clinical Medicine, Nanjing Medical University, 138 Han Zhong Road, Nanjing, Jiangsu 210029, P.R. China  
E-mail: jinyao1972@126.com

\*Contributed equally

**Key words:** retinal neurodegeneration, optic nerve transection, metabolomics, biomarker

been found to be associated with RGC degeneration, ranging from nucleic acids to proteins, such as microRNAs (14), long noncoding RNAs (15) and circular RNAs (16). However, the sensitivity, specificity and reliability of these biomarkers remain elusive and limit their applications in clinical practices.

As the ultimate products of the gene, mRNA and protein activity, the metabolites represent the most downstream stages of biological physiological and pathological processes (17). Metabolomics has been used for studying the dynamic changes of metabolites and metabolic pathways in response to external and internal stimuli (18) and identifying the biomarkers for disease prediction and therapeutic intervention. A growing number of metabolomics studies have been conducted in various types of cancer (19), neurological diseases (20) and cardiovascular diseases (21). Recent studies have revealed the obvious changes of metabolites in neurodegenerative diseases through the metabolomics analysis of cerebrospinal fluid, plasma, urine, saliva, and brain tissue from clinical samples or animal models. For example, Mapstone *et al* (22) reported that the changes in lipids and particularly phospholipids in plasma can identify amnesic mild cognitive impairment or Alzheimer's disease. The pathway enrichment data from the brain suggests that the dysfunction of taurine and hypotaurine metabolism, bile acid biosynthesis, serine and threonine metabolism or tricarboxylic acid cycle is tightly related to the onset and progression of Parkinson's disease (23). Lipid and sugar metabolism dysfunction is involved in the pathogenesis of neurodegenerative diseases (24).

The metabolomics analysis of ocular neurodegenerative diseases has also been conducted. The levels of several amino acids, acetoacetate, and citrate increase in the aqueous humor of chronic glaucoma rat model (25). Mitochondrial dysfunction, senescence and polyamines deficiency have been detected in the pathogenesis of glaucoma (26). Thus, altered retinal metabolites can lead to abnormal nutrient availability and impaired visual function.

At present, to the best of our knowledge, there is still no metabolomics study for the prediction of RGC degeneration based on retinal tissues, which can directly reflect the pathological condition of retinal neurodegeneration. The present study used untargeted metabolomics to investigate the changes of retinal metabolomic profiles following ONT injury in a mouse model.

## Materials and methods

**Animal experiment and ethical statement.** C57BL/6J mice (age, 8 weeks old; male; weight, 22–25 g) were obtained from the Animal Core Facility of Nanjing Medical University (Nanjing, China). All experiments were approved by the Animal Ethics and Experimentation Committee of Nanjing Medical University (approval no. 2103027). The animals were treated according to the ARVO Statement for the Use of Animals in Ophthalmic and Vision Research and housed with a 12 h light/12 h dark cycle with standard chow and water *ad libitum* under the controlled environment (temperature, 25°C; humidity, 50%). A total of 80 animals were used in this study.

**Optic nerve transection.** The mice were anesthetized with an intraperitoneal injection of the mixture of ketamine

(100 mg/kg) and xylazine (10 mg/kg) and the eyes were topically anesthetized with 0.5% proparacaine hydrochloride. The optic nerve was accessed within the ocular orbit via an incision in the tissue covering the superior border of orbital bone. The eye muscle and orbital fat was bluntly dissected above the eyeball. The optic nerve was disclosed through the orbital muscle cone and transected 2 mm posterior to the eyeball with a pair of jeweler forceps. The cut site was thoroughly examined to ensure that the optic nerve was completely cut. The fundus was examined fundoscopically to confirm the absence of injuries to retinal vascular supply. After the surgery, erythromycin eye ointment was applied to prevent further infection.

**Retinal whole-mount immunofluorescence.** At 7 days following building ONT model, the mice were anesthetized with an intraperitoneal injection of the mixture of ketamine (100 mg/kg) and xylazine (10 mg/kg). Euthanasia was performed by cervical dislocation when the animals were under deep anesthesia. Then, the eyes were fixed in 4% paraformaldehyde (PFA; cat. no. BL539A; Biosharp Life Sciences) for 30 min at room temperature and dissected into the petal shape as a whole-mount. Following incubation in 0.2% Triton-X-100 at 4°C overnight and 5% BSA for 1 h, the intact retina was incubated with anti- $\beta$ -III tubulin (Tuj1) antibody (1:400; cat. no. 801201; BioLegend, Inc.) overnight at 4°C. Following washing with PBS buffer, the retinas were incubated with Alexa Fluor 594 goat anti-mouse IgG (1:500; cat. no. A11005; Invitrogen; Thermo Fisher Scientific, Inc.) antibody for 2 h at room temperature. The representative images were captured from the peripheral areas of the retinas using a fluorescence microscope (x400 magnification; Olympus IX-73; Olympus Corporation). To evaluate RGC survival, four regions were randomly selected for each retina. The number of Tuj1<sup>+</sup> cells was counted using ImageJ software (version 1.8.0; National Institutes of Health) and averaged. The survival rate of RGCs was presented as the percentage of the number of Tuj1<sup>+</sup> cells in the injured retina compared with that in the uninjured retina.

**Hematoxylin and eosin (HE) staining.** At day 7 following building ONT model, euthanasia was performed by cervical dislocation when the animals were under deep anesthesia with the mixture of ketamine (100 mg/kg) and xylazine (10 mg/kg). The eyeballs were immediately enucleated and fixed in the Fekete's solution for 3 h at room temperature and the optic nerves were fixed in 4% PFA at 4°C overnight. Then, the optic nerves were dehydrated using gradient ethanol, embedded in paraffin and sliced into 5  $\mu$ m thickness. To observe the structural changes of axons, the longitudinal sections were deparaffinized with xylene, rehydrated through a graded ethanol series, and stained with hematoxylin and eosin (H&E; BP-DL001; Nanjing SenBeiJia Biological Technology Co., Ltd.). The sections were observed using a light microscope (x400 magnification; Olympus IX-73; Olympus Corporation) equipped with a DP80 camera.

**Sample collection and preparation.** ONT model was induced in the left optic nerve and the contralateral eye served as the control. On the day 7 following ONT injury, the mice were euthanized and the retinas were harvested. The pooled retinas from the ipsilateral eyes of five mice was taken as a sample.

Approximately 7 mg of retinal sample was subsequently vortexed in 200  $\mu$ l methanol/H<sub>2</sub>O (4/1, vol/vol) cold solvent, containing 10  $\mu$ l of 2-chlorophenylalanine (0.06 mg/ml) as the internal standard. After grinding at 60 Hz and -20°C for 2 min, each retinal sample was sonicated at 40 KHz in an ice-water bath for 10 min at 0°C and then centrifuged at 4°C (15,620 x g) for 10 min. The supernatant of each sample was dried with a freeze-concentration centrifugal dryer and dissolved in 190  $\mu$ l of methanol/H<sub>2</sub>O (4/1, vol/vol) solvent at 4°C for 30 sec. After that, the samples were sonicated at 40KHz in an ice-water bath at 0°C for 3 min and centrifuged at 4°C (15,620 x g) for 10 min, followed by the collection through a crystal syringe and filtration through a 0.22  $\mu$ m microfilter into LC vials. The vials were stored at -80°C before analysis. The quality control (QC) samples were prepared by mixing the aliquots from all retinal samples.

**Liquid-chromatography tandem mass spectrometry (LC-MS/MS) analysis.** Metabolic profiling was performed using the ACQUITY UPLC I-Class plus system (Waters Corporation) coupled with Q-Exactive plus quadrupole-Orbitrap mass spectrometer (Thermo Fisher Scientific, Inc.) in both positive ion and negative ion modes of electrospray ionization (ESI). In brief, ultra-performance liquid chromatography separation was performed on an ACQUITY UPLC HSS T3 column (100x2.1 mm; 1.8  $\mu$ m) at 45°C. Gradient elution was performed using (A) water (0.1% formic acid) and (B) acetonitrile (0.1% formic acid) as the mobile phase with an injection volume of 5  $\mu$ l and a flow rate of 0.35 ml/min, starting at 95% A for 2 min and decreasing to 20% within 8 min. Next, the gradient decreased to 0 within 4 min and kept for 1 min, and then increased to 95% within 0.1 min and kept for 1 min.

The sample mass spectrum signals were collected in the positive and negative ion scanning modes. The scanning range was from 100 to 1,200 mass-to-charge ratio (m/z). The resolution was set at 70,000 in the full scan mode and 17,500 in the HCD MS/MS scan model. The aux gas and sheath flow rates were 10 and 40 arbitrary units, respectively. The nitrogen gas temperature was 350°C. The spray voltages were set to 3800 V(+) and 3200 V(-). QCs were added periodically to assess the repeatability.

**Metabolomics data analysis.** Software Progenesis QI V2.3 (Nonlinear Dynamics) was used to handle raw peak extraction, baseline filtering, retention time correction, peak alignment, peak identification and normalization. The compounds were identified based on m/z, secondary fragments and isotopic distribution. They were then characterized using the Human Metabolome Database (HMDB; <https://hmdb.ca/>), Metlin (<https://metlin.scripps.edu>), Lipidmaps (V2.3) (<https://www.lipidmaps.org/>) and EMDB2.0 (27). EMDB2.0 database is a local mass spectrometry database established by Lu-ming Biotechnology through standardized methods and standards, covering over 2,000 common metabolites. The extracted data were then processed by removing the peaks with a missing value (ion intensity=0) in >50% in groups, replacing 0 value by half of the minimum value, and screening according to the qualitative results of the compound. Compounds with the resulting scores below 36 (out of 60) points were also deemed to be inaccurate and removed. A data matrix was combined

from the positive and negative ion data. Principal component analysis (PCA) was performed to reduce data dimensionality and visualize the relationship among samples. Orthogonal Partial Least-Squares-Discriminant Analysis (OPLS-DA) was applied for multivariate statistical analysis to identify the differential metabolites. To assess the quality of a model, 7-fold cross-validation and 200 Response Permutation Testing were conducted to prevent overfitting. A two-sided unpaired Student's t-test was used to calculate the statistical significance and fold-change of the metabolites. The relative importance of each metabolite to the OPLS-DA model was evaluated by the parameter, variable importance in projection (VIP). The metabolites with P<0.05 and VIP  $\geq$ 1 were considered as the differential metabolites for group discrimination.

The impact pathway was determined using the Pathway Analysis Module of MetaboAnalyst 5.0 (<http://www.metaboanalyst.ca/>) based on the Kyoto Encyclopedia of Genes and Genomes (KEGG) pathway library (<https://www.kegg.jp/>), with the criteria as P<0.05, false discovery rate (FDR) <0.05 and impact >0.05. Before MetaboAnalyst analysis, the sample was normalized by the median and the data was log<sub>10</sub>-transformed for comparison. The parameters were as follows: 'Scatter plot' visualization method, 'global test' enrichment method, 'relative-betweenness centrality' topology analysis and reference metabolome of all compounds in the selected pathway library of '*Mus musculus* (KEGG)'.

The areas under the receiver operating characteristic (ROC) curves (AUC) analysis was performed using the Biomarker Analysis Module of MetaboAnalyst 5.0 to assess the predictive capacities of the potential biomarkers with an AUC of >0.8 as the potential markers. Before MetaboAnalyst analysis, the sample was normalized by the median. The data was log<sub>10</sub>-transformed for comparison and auto-scaled (mean-centered and divided by the standard deviation of each variable). The 95% confidence intervals were calculated using 500 bootstrappings. For multivariate ROC analysis, the linear support vector machine algorithm was used to evaluate the combined biomarker model of the selected metabolites via ROC curve based model evaluation (Tester) section. 100 cross-validation were performed and the results were averaged to generate the plot.

**Statistical analysis.** Statistical analysis was performed using GraphPad Prism 8 software (Dotmatics). All data were expressed as the mean  $\pm$  SD. For normally distributed data, an unpaired Student's t-test was used for pairwise comparisons. For non-normally distributed data, Mann-Whitney U test was performed for pairwise comparisons. P<0.05 was considered to indicate a statistically significant difference.

## Results

**Establishment of murine ONT model.** The untargeted metabolomics was used to detect the changes of retinal metabolomic profile in the ONT model. The experimental flow of metabolomics analysis is presented in Fig. 1A. To confirm the successful establishment of the ONT model, the whole-mounted retinas were stained with TuJ1 to detect the survival of RGCs at day 7 following ONT injury. The results showed that ONT injury led to a ~50% decrease in the number of survival RGCs (Fig. 1B).

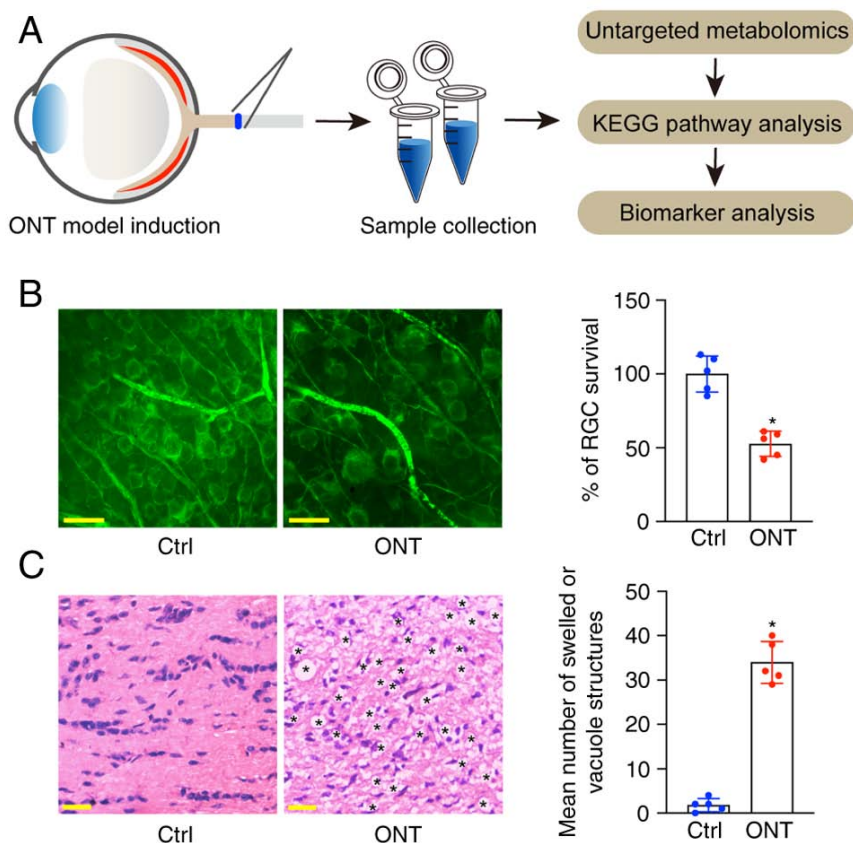


Figure 1. Establishment of murine ONT model. (A) Flowchart of the experimental design. (B) Fluorescent images of the retinas stained with anti-Tuj1 antibody were observed from the peripheral areas. The percentage of surviving RGCs were detected by calculating the average number of Tuj1<sup>+</sup> cells in the area of the injured retina compared with that in the normal retina. The representative images are shown (n=5; scale bar, 20  $\mu$ m). (C) Hematoxylin and eosin staining was conducted to detect the degeneration of myelin sheath in the injured optic nerves (n=5; scale bar, 20  $\mu$ m). \*P<0.05 vs. Ctrl. ONT, optic nerve transection; RGC, retinal ganglion cells; KEGG, Kyoto Encyclopedia of Genes and Genomes; Ctrl, control; Tuj1,  $\beta$ -III tubulin.

H&E staining of the longitudinal sections revealed that the axons in the normal group were well organized and the optic nerve fibers were intact. By contrast, the axons in ONT injured group were swollen and contained vacuole structures (Fig. 1C). The aforementioned results indicated that the building of ONT model was successful.

**Untargeted metabolomic profile of retinal tissues of ONT mice and non-ONT controls.** To reveal the global metabolomic profile change following ONT injury, a total of 12 retinal samples were collected from six ONT retinas and six non-ONT retinas. A total of 2,928 anionic peaks and 3,745 cationic peaks of metabolites were recorded. Two-dimensional and three-dimensional PCA models with the score plots indicated that ONT samples clustered together, while the non-ONT Ctrl samples clustered together, indicating that the experiments displayed good repeatability (Fig. 2A and B). Next, OPLS-DA model with the supervised method was constructed to determine the metabolomic profile differences for the separation of two groups. As shown in Fig. 2C, separations of ONT group and non-ONT control group were observed, with the model values of R2X (cum)=0.688, R2Y (cum)=0.939, and Q2 (cum)=0.93. In addition, the permutation analysis showed that the R<sup>2</sup> value was lower compared with the original value. The Q<sup>2</sup> intercept was negative, indicating that there was no sign of overfitting,

which ensured the validity and stability of the OPLS-DA model fitting (Fig. 2D).

**Identification of altered metabolites and metabolic pathways following ONT injury.** A volcano plots was used to calculate the fold-change and P-value of all metabolites for the identification of altered metabolites following ONT injury. VIP was used to measure the effects of metabolite expression patterns on the classification and discrimination of the samples in each group. The results showed 689 differential metabolites were identified according to the threshold of P<0.05 and VIP>1 (Fig. 3A), including lipids and lipid-like molecules (36.57%), organic acids and derivatives (12.19%), organic oxygen compounds (7.69%), organoheterocyclic compounds (7.26%), nucleosides, nucleotides, and analogues (4.64%), phenylpropanoids and polyketides (2.61%), benzenoids (1.89%), organic nitrogen compounds (1.16%), alkaloids and derivatives (0.58%), homogeneous non-metal compounds (0.29%), lignans, neolignans and related compounds (0.15%), organosulfur compounds (0.15%), and unclassified (24.82%) (Fig. 3B).

KEGG analyses were then carried out to determine the involvement of the signaling pathways of altered metabolites following ONT injury. The results revealed that 122 metabolites were annotated and enriched in 50 KEGG pathway databases (Table SI). A total of 25 metabolic pathways were identified with P<0.05 and impact >0.05. As demonstrated



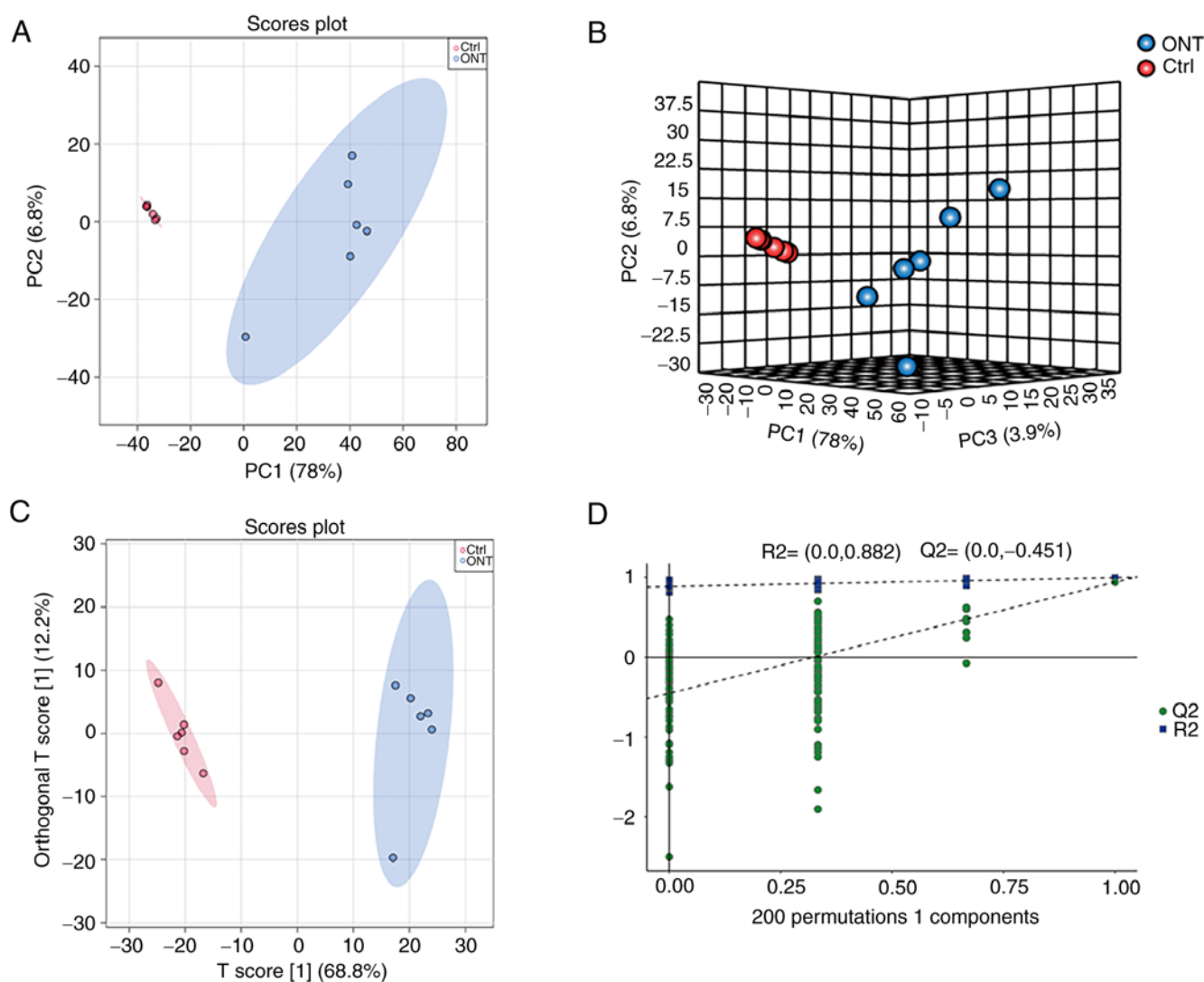


Figure 2. Untargeted metabolomic profile of retinal tissues of ONT mice and non-ONT controls. (A) Two-dimensional PCA score plot of ONT group and non-ONT control group. (B) Three-dimensional PCA score plot of ONT group and non-ONT control group. (C) OPLS-DA score plot of ONT group and non-ONT control group. (D) 200 response permutation analysis plot of OPLS-DA model. ONT, optic nerve transection; PCA, principal component analysis; OPLS-DA, Orthogonal Partial Least-Squares-Discriminant Analysis; Ctrl, control.

in Fig. 4A, the top 10 enriched pathways were: i) 'Primary bile acid biosynthesis'; ii) 'Fructose and mannose metabolism'; iii) 'Pentose phosphate pathway'; iv) 'Sphingolipid metabolism'; v) ' $\beta$ -Alanine metabolism'; vi) 'Riboflavin metabolism'; vii) 'Arginine biosynthesis'; viii) 'Steroid hormone biosynthesis'; ix) 'Phenylalanine, tyrosine and tryptophan biosynthesis'; and x) 'Tyrosine metabolism'. The impact factors were 0.07, 0.16, 0.17, 0.08, 0.06, 0.5, 0.23, 0.05, 0.5 and 0.14, respectively. As demonstrated in Fig. 4B, 20 altered metabolites were identified in the aforementioned 10 metabolic pathways, including 13 upregulated metabolites and 7 downregulated metabolites in ONT retinal tissues (Table SII).

**Potential biomarkers for ONT injury.** Lipids are the major macromolecule in the brain, accounting for 50% of dry brain weight (28). The lipid content of CNS is only lower compared with that in adipose tissue. Moreover, altered lipid metabolism has been proven to be involved in the pathogenesis of neurodegenerative diseases (29).

Among the altered metabolic pathways following ONT injury, the primary bile acid biosynthesis and sphingolipid metabolism are the key pathways affecting lipid metabolism. To screen for the metabolites as the candidate markers for ONT injury, the present study investigated the altered metabolites enriched in these two pathways. As demonstrated in Fig. 5A, three altered metabolites were chosen as the candidate biomarkers in the primary bile acid biosynthesis pathway, including taurine, taurochenodesoxycholic acid and taurocholic acid (TCA). The P-values were  $7.16 \times 10^{-6}$ ,  $4.79 \times 10^{-4}$ , and 0.0083, respectively. AUC-ROC was used to detect the possibility of these metabolites as the candidate biomarkers. The results showed the AUC values of these biomarkers were 1 (Fig. 5B-D). The levels of taurochenodesoxycholic acid and TCA were significantly increased following ONT injury, while the level of taurine was significantly decreased following ONT injury. Next, the multivariate biomarker model was used by applying these three metabolites for ROC analysis to test whether the primary bile acid biosynthesis was sufficient to distinguish ONT group from non-ONT control group. The result also showed that the value of AUC was 1 (Fig. 5E).

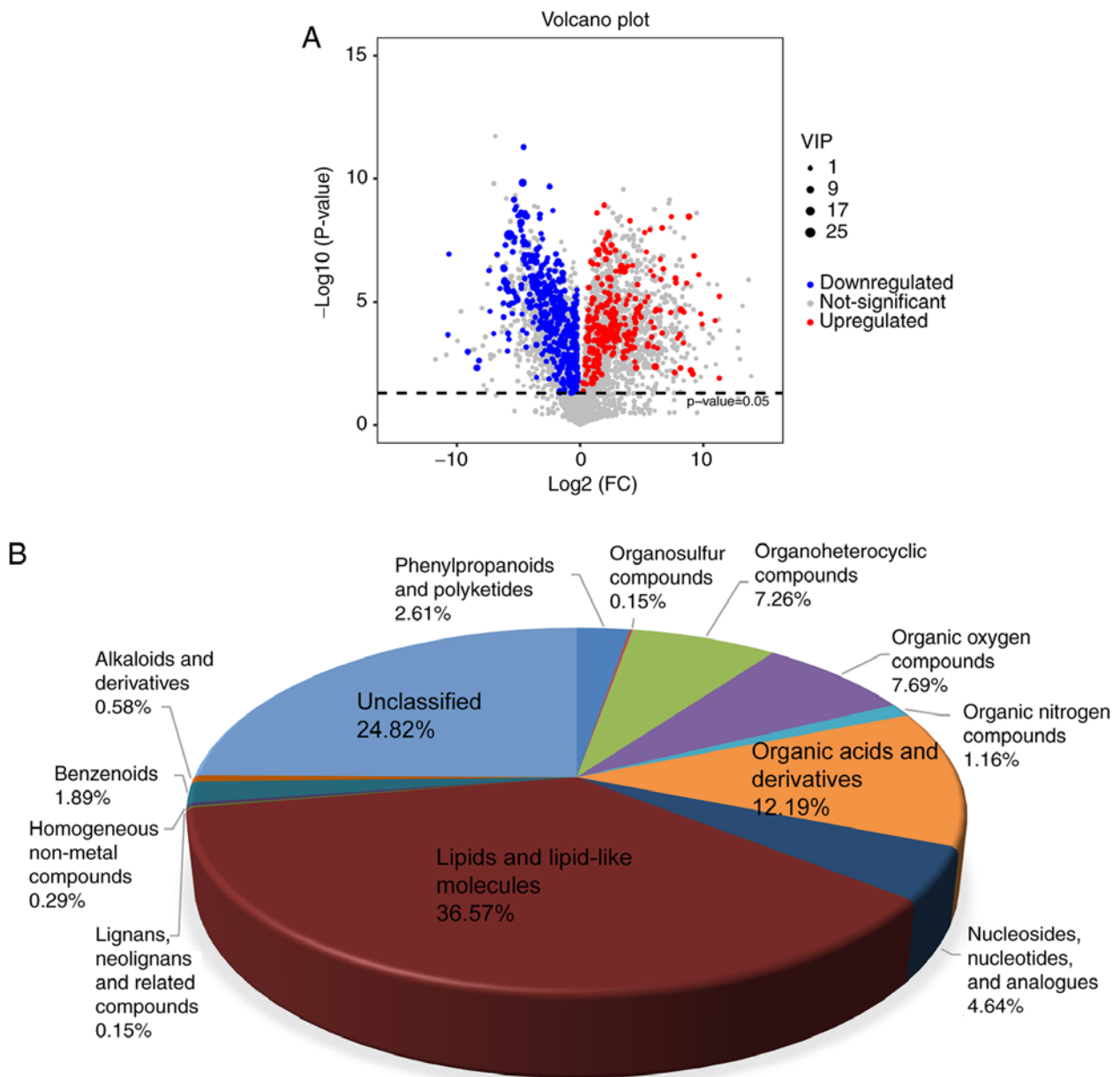


Figure 3. Identification of altered metabolites following ONT injury. (A) Volcano plot analysis was conducted to identify the altered metabolites following ONT injury according to the criteria ( $P < 0.05$  and  $VIP > 1$ ). Red and blue represent the upregulated and downregulated metabolites, respectively. (B) Pie chart shows the differential expressed metabolites between ONT group and non-ONT control group. ONT, optic nerve transection; VIP, variable importance in projection.

As shown in Fig. 6A, two metabolites, sphingosine and galabiosylceramide (d18:1/16:0), were selected as the candidate biomarkers of sphingolipid metabolism pathway, with P-values of 0.0010 and 0.0026, respectively. The level of sphingosine was significantly increased following ONT injury. By contrast, the level of galabiosylceramide (d18:1/16:0) was decreased following ONT injury. ROC analysis showed that the AUC values of these two metabolites were 1 (Fig. 6B and C). The multivariate biomarker model also showed the value of AUC was 1 (Fig. 6D).

## Discussion

RGCs serve as the connecting ring between the neuroretina and the sensory retina. Their axons can form optic nerve and bring the visual input to the brain (4). Once the axons

pass through the lamina cribrosa, they are surrounded by the myelin, thereby accelerating the transmission speed of neurons. However, due to the limitation in the length, trajectory and space, the axons are highly susceptible to external damage (30). RGC loss has been recognized as the hallmark of neurodegenerative diseases. Several animal models of RGC degeneration have been established, which can be induced by ocular hypertension (injection of saline/silicon oil/hyaluronic acid into the eyes, episcleral vein occlusion, pressure-induced retinal ischemia/reperfusion, and inbred DBA/2J mice) (31), mechanical stress (optic nerve compression/transection and ocular blast) (12,14), and glutamate neurotoxicity (intravitreal injection of N-methyl-D-aspartate, glutamate transporter or specific NMDAR deficit mice) (1). However, the injury sites in these models are not identical.

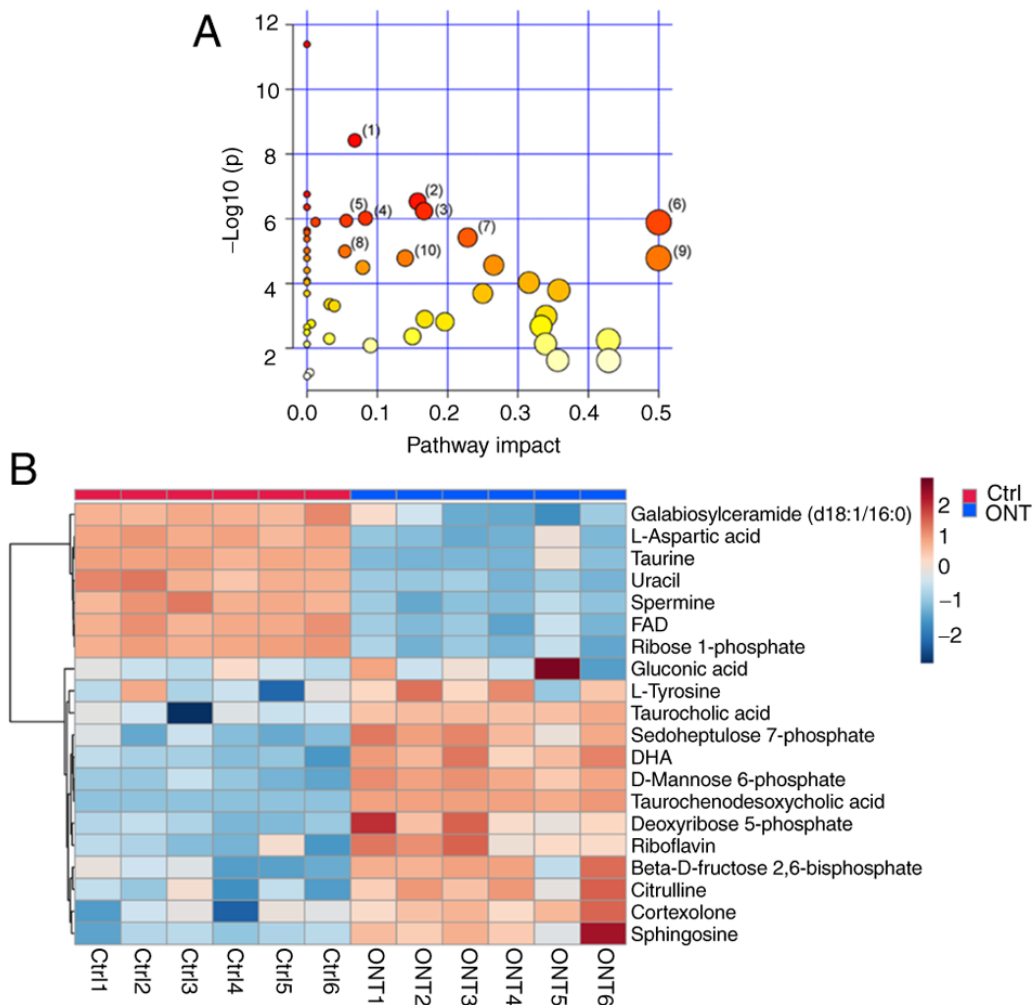


Figure 4. Identification of altered metabolic pathways following ONT injury. (A) Pathway enrichment and topology analysis. The size of the bubble indicates the pathway impact value. The vertical coordinate and color of the bubble indicate the P-value. (B) Heatmap of 20 altered metabolites in the aforementioned 10 pathways. Blue indicates relative low levels of each metabolite and red indicates relative high levels of each metabolite. ONT, optic nerve transection; Ctrl, control.

The optic nerve is composed of fibers projecting to the brain from the neuronal RGCs, whose cell bodies are located in the retina. Ocular hypertension and glutamate neurotoxicity primarily leads to an obvious injury to RGC axons and somas, which is intraretinal (1,32). However, optic nerve injury in the models of mechanical stress is extraretinal. Following optic nerve injury, the injury signals travel retrogradely to RGC somata located in the retina, eventually causing RGC degeneration (33). Thus, mechanical stress models are important models for studying the mechanism of RGC degeneration following extraretinal injury.

Notably, the animal models mimicking mechanical injury mainly include optic nerve crush (ONC) and ONT models (34). ONC is generally less severe compared with ONT and can be used to determine axon regeneration across the lesion sites. However, the differences in crush force and duration can affect tissue responses and lesions, resulting in the difficulty in replication and bias in the identification of potential biomarkers. ONT is a model of RGC degeneration through direct injury of RGC fibers, ensuring that the severity of injury in the experimental individuals is consistent (35).

The present study thus selected an ONT model for studying retinal neurodegeneration. ONT can cause rapid degeneration of RGCs due to the loss of trophic support. In an ONT model, axonal injury directly damages the axolemma, immediately exposing the injured axonal cylinder to extracellular environment and causing the influx of sodium and calcium (36). The resultant calcium-dependent cysteine protease called calpain is activated in the later stage of axonal degeneration, which degrades the axons and causes neuronal death (37). Similarly to other CNS in the higher vertebrates, optic nerve axon damage can cause the loss of RGCs, resulting in irreversible vision impairment. Hence, functional recovery of vision requires restoring the functions of injured RGCs (38). However, the exact mechanism of RGC degeneration remains unclear. Metabolomics has been widely used to investigate the mechanism and identify the metabolic signatures of disease progression (39). The untargeted metabolomics can obtain the comprehensive reads of the detailed analyses of detected metabolites (40). Thus, identifying the metabolic signature of RGC degeneration can provide novel insights into the identification of potential drug targets for treating retinal neurodegeneration.

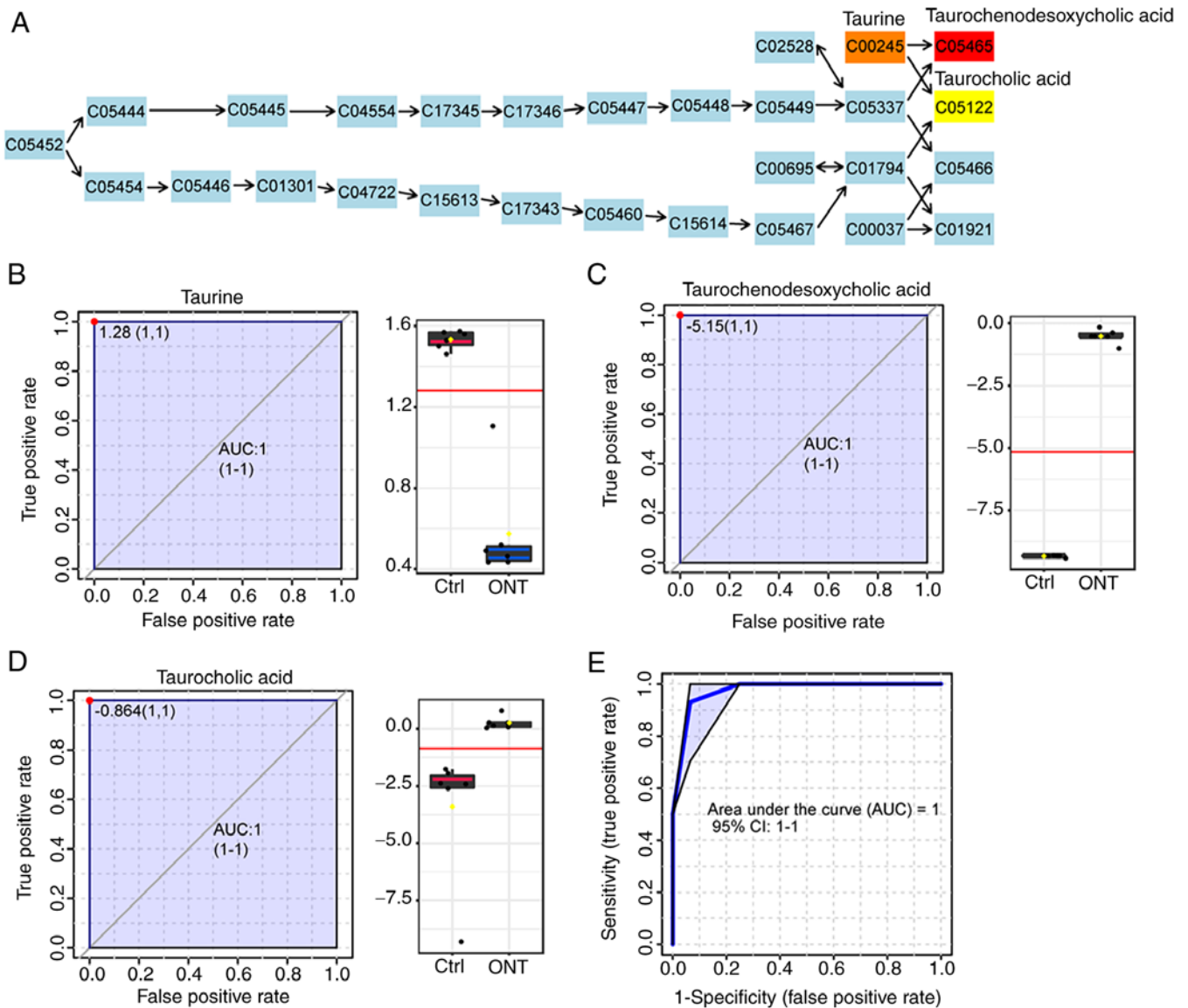


Figure 5. Multivariate analysis of primary bile acid biosynthesis. (A) Graphical presentation of KEGG signaling map of primary bile acid biosynthesis. Blue indicates the metabolites used as background; red, orange, and yellow indicate the metabolites with different levels of significant variability between ONT group and non-ONT ctrl group. ROC curve of the metabolites from primary bile acid biosynthesis: (B) Taurine, (C) Taurochenodesoxycholic acid and (D) TCA. (E) ROC curve of primary bile biosynthesis (combination of taurine, taurochenodesoxycholic acid and TCA) following ONT injury. ONT, optic nerve transection; KEGG, Kyoto Encyclopedia of Genes and Genomes; ROC, receiver operating characteristic; TCA, taurocholic acid; Ctrl, control; AUC, area under the curve.

LC-MS/MS technology was used to screen for the altered metabolites following ONT injury. The metabolomics profiles were conducted between ONT retinas and non-ONT retinas and 689 differential metabolites were identified. The metabolite pathways, including primary bile acid biosynthesis and sphingolipid metabolism related to lipid metabolism, were altered following ONT injury. A total of five metabolites were identified as the candidate biomarkers for retinal neurodegeneration. In addition, altered amino acids and glucose metabolism were observed in the retinas following ONT injury.

The present study also observed that lipids and lipid-like molecules were mainly involved in the altered metabolite pathways following ONT injury, suggesting that lipids exert imperative effects on the progression of ONT injury, which confirmed the association between lipid metabolism and neurodegeneration (28). As the major components of the

bilayer membrane, lipids exert imperative effects in maintaining normal physiological functions of CNS, including energy production and cell-to-cell signal transduction (41). Damaged neurons require large amounts of lipids to form the membranes during regeneration (42). A previous study has revealed that lipin1, a critical regulator of glycerolipid metabolism in neurons, can enhance axon regeneration after optic nerve injury (43).

Subsequently, the altered metabolites following ONT injury were annotated using KEGG, HMDB, Lipidmaps (V2.3), Metlin and EMBD2.0. These altered metabolites following ONT injury were highly enriched in 50 metabolite pathways. Among the top 10 metabolic pathways, 'fructose and mannose metabolism' (44), 'pentose phosphate' (45), 'β-Alanine metabolism' (46), 'arginine biosynthesis' (47), 'sphingolipid metabolism' (48) and 'steroid hormone biosynthesis' (49) are



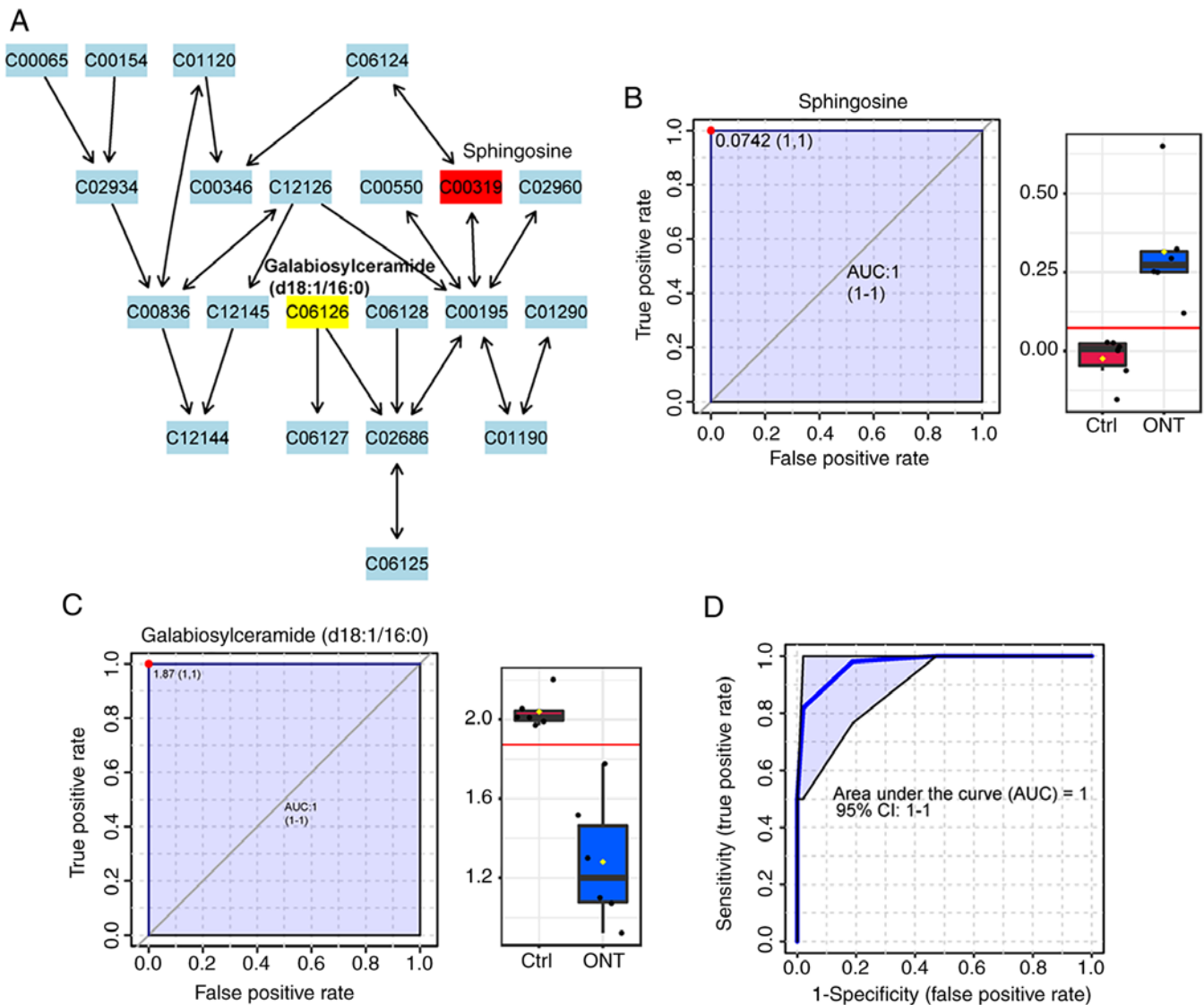


Figure 6. Multivariate analysis of sphingolipid metabolism. (A) Graphical presentation of KEGG signaling map of sphingolipid metabolism. Blue indicates the metabolites used as background; red and yellow indicate the metabolites with different levels of significant variability between the two groups. ROC curve of the metabolites from sphingolipid metabolism: (B) Sphingosine, (C) Galabiosylceramide (d18:1/16:0). (D) ROC curve of the metabolites from primary bile biosynthesis pathway [combination of sphingosine and galabiosylceramide (d18:1/16:0)] following ONT injury. KEGG, Kyoto Encyclopedia of Genes and Genomes; ROC, receiver operating characteristic; Ctrl, control; AUC, area under the curve.

involved in the pathogenesis of diabetic retinopathy. Altered 'sphingolipid metabolism' (50), 'tyrosine metabolism' (51) and 'steroid hormone biosynthesis' (52) have been found in the pathogenesis of glaucoma. Altered 'arginine metabolism' has been detected between Vogt-Koyanagi-Harada and healthy controls (53). The metabolites of primary bile acid biosynthesis are tightly associated with the pathogenesis of age-related macular degeneration (54). Riboflavin deficiency can cause severe decreases in retinal function accompanied by structural changes in the neural retina and retinal pigment epithelium (55). Among these altered pathways, 'primary bile acid biosynthesis' and 'sphingolipid metabolism' are tightly associated with lipid metabolism and involve several pathological processes, such as inflammation, neovascularization, survival and death of neurons and migration of endothelial cells (54,56).

Primary bile acid biosynthesis is a crucial pathway for cholesterol catabolism and homeostasis maintenance (57).

Primary bile acid is synthesized from cholesterol in the liver and converted to secondary bile acid by anaerobic bacteria in the gut. Finally, bile acid is reabsorbed by enterocytes and transited back to the liver via the portal vein to produce glycine and taurine (58). Dysfunction of bile acid biosynthesis is involved in the onset and progression of Parkinson's disease (23). In addition, a previous study has revealed that patients with Alzheimer's disease have lower levels of serum primary bile acids compared with the normal healthy controls (58). The present study detected the differential expression of taurine, taurochenodesoxycholic acid and TCA following ONT injury. ROC curve analysis indicated that these altered metabolites could be selected as the candidate biomarkers for detecting retinal neurodegeneration. Taurine, a sulfur-containing amino acid, is reduced by 76.29% in the ONT group (59,60). Taurochenodesoxycholic acid and TCA are increased in concentrations following optic nerve injury. Taurine is highly expressed in the mammalian brain, heart and leukocytes, and

is one of the most abundant amino acids (61). Taurine plays protective roles in diverse CNS disorders by regulating intracellular calcium transport, affecting antioxidation and acting as a neuroprotector against L-glutamate-induced neurotoxicity (62,63). Additionally, treatment with taurine can suppress NMDA-induced retinal cell apoptosis by reducing oxidative stress (64).

Taurochenodesoxycholic acid and TCA have been reported to be the highest bile acid in the serum of the patients with cirrhosis (65). Taurochenodesoxycholic acid, the conjugate of taurine and bile acid, exerts its anti-inflammatory and immunomodulatory functions and enhances apoptosis via the activation of PKC-c-JNK/P38 signaling (66). The significant upregulation of taurochenodesoxycholic acid in ONT group may be associated with the activation of inflammatory response and apoptosis of RGCs following ONT injury. TCA (a major 12 $\alpha$ -hydroxylated bile acid), composed of taurine and cholic acid, is significantly increased in the ONT group (67). Even though its roles in neurodegeneration have not yet been elucidated, previous studies reported the altered plasma levels of bile acids in patients with AMD, demonstrating a protective effect of TCA on both degeneration and neovascular AMD (54). Moreover, plasma levels of TCA are tightly related to inflammatory biomarkers in patients coinfecting with human immunodeficiency virus/hepatitis C virus (68). As an upstream compound of taurochenodesoxycholic acid and TCA, taurine is becoming a promising target for reversing the disorders caused by axonal injury.

Sphingolipid is highly expressed in myelin sheaths and plays important roles in maintaining neuronal survival, signal transduction and synaptic stability (69). Abnormal sphingolipid metabolism occurs in several CNS diseases (70). Altered sphingolipid metabolism due to Golgi-associated retrograde protein (GARP) mutations contributes to neurodegeneration, and inhibitor of sphingolipid synthesis can greatly improve the outcomes and survival in GARP mutant wobbler mice (a model of motor neuron degeneration) (71). Sphingolipid metabolites, particularly sphingosine-1-phosphate and ceramide, are crucial for the proliferation, survival and activation of astrocytes, microglia and neurons (72,73). The present study observed higher levels of sphingosine and lower levels of galabiosylceramide (d18:1/16:0) in the ONT group compared with those in the control group. Furthermore, the combination of these two metabolites showed good sensitivity and specificity. Altered patterns of lipid metabolism and apoptosis through ceramide pathways have been reported in another metabolomics study targeting 195 metabolites (74).

Sphingosine consists of hydrophobic sphingoid long-chain bases and can be converted to sphingosine-1-phosphate by sphingosine kinase (75). Increased levels of sphingosine have also been detected in the patients with primary open-angle glaucoma based on an untargeted plasma metabolomic study (76). This study suggests that axonal injury-induced excessive sphingosine may be involved RGC degeneration through ceramide apoptosis signaling. However, no difference was detected in sphingosine-1-phosphate level in the ONT group in the present study, which differed from another study on Parkinson's disease (77). The study consistency and differences present the opportunities for further metabolic in retinal neurodegenerative diseases. Galabiosylceramide (d18:1/16:0),

the last unit of glycosphingolipids, decreased by 62.5% after axonal injury in the present study. Although the mechanism of galabiosylceramide (d18:1/16:0) remains unknown, it may serve as a potential biomarker of retinal neurodegeneration to some extent.

There are still some limitations in the present study. A relatively typical sampling time was selected. The potential impacts of sampling time points on retinal metabolic profile should be further considered. Although the present study predicted the involvement of altered metabolite pathways following ONT injury, the potential mechanism associated with the altered pathways and metabolites in ONT and retinal neurodegeneration remains unclear and requires further study. In addition, the key metabolic enzymes, including bile acid-CoA:amino acid N-acyltransferase (78,79), Acyl-coenzyme A amino acid N-acyltransferase 1 (80), acid ceramidase, neutral ceramidase, alkaline ceramidase (81), sphingosine-1-phosphate phosphatase (82) and phospholipid phosphatase, which are in charge of the production of these altered metabolites, should be analyzed in the further research (83). To identify the reliable biomarkers for the diagnosis of retinal neurodegeneration, the targeted metabolomics should also be conducted on the clinical samples.

In conclusion, the present study identified the changes of metabolomic profile in retinal tissues of ONT mice via LC-MS/MS analysis. A total of 689 differential metabolites and 50 altered metabolic pathways were identified following ONT injury. The major types of altered metabolites were lipids and lipid-like molecules, suggesting that lipid-related metabolism was tightly associated with the process of retinal neurodegeneration. Primary bile acid biosynthesis pathway, sphingolipid metabolism pathway and five altered metabolites with high sensitivity and specificity (AUC>0.8) were identified following ONT injury. The levels of taurochenodesoxycholic acid, TCA and sphingosine increased, while the levels of taurine and galabiosylceramide decreased in the ONT model, implying that these altered metabolites are the potential therapeutic target for ONT injury. The present study may provide novel insights into the pathogenesis of RGC degeneration and provide the candidate metabolic targets for the diagnosis and treatment of retinal neurodegenerative diseases.

## Acknowledgements

Not applicable.

## Funding

This study was supported by the National Natural Science Foundation of China (grant nos. 82225013, 82171074 and 81970809) and the Shanghai Youth Talent Support Program (grant no. 2016).

## Availability of data and materials

Raw datasets for metabolic profiling have been deposited to the MetaboLights Repository ([www.ebi.ac.uk/metabolights/MTBLS7911](http://www.ebi.ac.uk/metabolights/MTBLS7911)) with the Study Identifier MTBLS7911. Other datasets used and/or analyzed during the current study available from the corresponding author on reasonable request.

## Authors' contributions

BY and JY designed this study. JZ, XN, SL and YJ performed the experiments, figure preparation and manuscript draft. JZ, XN and XH developed the methods and performed data analysis. JZ and XN acquired and interpreted the data. JZ and BY wrote and revised the paper. JZ and JY confirm the authenticity of all the raw data. All authors read and approved the final manuscript.

## Ethics approval and consent to participate

All experiments were approved by the Animal Ethics and Experimentation Committee of Nanjing Medical University (approval no. 2103027).

## Patient consent for publication

Not applicable.

## Competing interests

The authors declare that they have no competing interests.

## References

- Guo X, Zhou J, Starr C, Mohs EJ, Li Y, Chen EP, Yoon Y, Kellner CP, Tanaka K, Wang H, *et al*: Preservation of vision after CaMKII-mediated protection of retinal ganglion cells. *Cell* 184: 4299-4314.e12, 2021.
- Parisi V, Oddone F, Ziccardi L, Roberti G, Coppola G and Manni G: Citicoline and retinal ganglion cells: Effects on morphology and function. *Curr Neuroparmacol* 16: 919-932, 2018.
- Levin LA and Gordon LK: Retinal ganglion cell disorders: Types and treatments. *Prog Retin Eye Res* 21: 465-484, 2002.
- Fry LE, Fahy E, Chrysostomou V, Hui F, Tang J, van Wijngaarden P, Petrou S and Crowston JG: The coma in glaucoma: Retinal ganglion cell dysfunction and recovery. *Prog Retin Eye Res* 65: 77-92, 2018.
- Jiang S, Kametani M and Chen DF: Adaptive immunity: New aspects of pathogenesis underlying neurodegeneration in glaucoma and optic neuropathy. *Front Immunol* 11: 65, 2020.
- Bojceviski J, Stojic A, Hoffmann DB, Williams SK, Muller A, Diem R and Fairless R: Influence of retinal NMDA receptor activity during autoimmune optic neuritis. *J Neurochem* 153: 693-709, 2020.
- Almasieh M, Wilson AM, Morquette B, Cueva Vargas JL and Di Polo A: The molecular basis of retinal ganglion cell death in glaucoma. *Prog Retin Eye Res* 31: 152-181, 2012.
- Wert KJ, Velez G, Kanchustambham VL, Shankar V, Evans LP, Sengillo JD, Zare RN, Bassuk AG, Tsang SH and Mahajan VB: Metabolite therapy guided by liquid biopsy proteomics delays retinal neurodegeneration. *EBioMedicine* 52: 102636, 2020.
- Lehtonen S, Sonninen TM, Wojciechowski S, Goldsteins G and Koistinaho J: Dysfunction of cellular proteostasis in Parkinson's disease. *Front Neurosci* 13: 457, 2019.
- Pardue MT and Allen RS: Neuroprotective strategies for retinal disease. *Prog Retin Eye Res* 65: 50-76, 2018.
- Tran AP, Warren PM and Silver J: The biology of regeneration failure and success after spinal cord injury. *Physiol Rev* 98: 881-917, 2018.
- Fung JCL and Cho EYP: Methylene blue promotes survival and GAP-43 expression of retinal ganglion cells after optic nerve transection. *Life Sci* 262: 118462, 2020.
- Tran NM, Shekhar K, Whitney IE, Jacobi A, Benhar I, Hong G, Yan W, Adiconis X, Arnold ME, Lee JM, *et al*: Single-cell profiles of retinal ganglion cells differing in resilience to injury reveal neuroprotective genes. *Neuron* 104: 1039-1055.e12, 2019.
- Mead B, Kerr A, Nakaya N and Tomarev SI: miRNA changes in retinal ganglion cells after optic nerve crush and glaucomatous damage. *Cells* 10: 1564, 2021.
- Ayupe AC, Beckedorff F, Levay K, Yon B, Salgueiro Y, Shiekhata R and Park KK: Identification of long noncoding RNAs in injury-resilient and injury-susceptible mouse retinal ganglion cells. *BMC Genomics* 22: 741, 2021.
- Wang JJ, Liu C, Shan K, Liu BH, Li XM, Zhang SJ, Zhou RM, Dong R, Yan B and Sun XH: Circular RNA-ZNF609 regulates retinal neurodegeneration by acting as miR-615 sponge. *Theranostics* 8: 3408-3415, 2018.
- Rinschen MM, Ivanisevic J, Giera M and Siuzdak G: Identification of bioactive metabolites using activity metabolomics. *Nat Rev Mol Cell Biol* 20: 353-367, 2019.
- Li Q, Wei S, Wu D, Wen C and Zhou J: Urinary metabolomics study of patients with gout using gas chromatography-mass spectrometry. *Biomed Res Int* 2018: 3461572, 2018.
- Yang QJ, Zhao JR, Hao J, Li B, Huo Y, Han YL, Wan LL, Li J, Huang J, Lu J, *et al*: Serum and urine metabolomics study reveals a distinct diagnostic model for cancer cachexia. *J Cachexia Sarcopenia Muscle* 9: 71-85, 2018.
- Shao Y and Le W: Recent advances and perspectives of metabolomics-based investigations in Parkinson's disease. *Mol Neurodegener* 14: 3, 2019.
- McGarrah RW, Crown SB, Zhang GF, Shah SH and Newgard CB: Cardiovascular metabolomics. *Circ Res* 122: 1238-1258, 2018.
- Mapstone M, Cheema AK, Fiandaca MS, Zhong X, Mhyre TR, MacArthur LH, Hall WJ, Fisher SG, Peterson DR, Haley JM, *et al*: Plasma phospholipids identify antecedent memory impairment in older adults. *Nat Med* 20: 415-418, 2014.
- Graham SF, Rey NL, Yilmaz A, Kumar P, Madaj Z, Maddens M, Bahado-Singh RO, Becker K, Schulz E, Meyerdirk LK, *et al*: Biochemical profiling of the brain and blood metabolome in a mouse model of prodromal Parkinson's disease reveals distinct metabolic profiles. *J Proteome Res* 17: 2460-2469, 2018.
- Botas A, Campbell HM, Han X and Maletic-Savatic M: Metabolomics of neurodegenerative diseases. *Int Rev Neurobiol* 122: 53-80, 2015.
- Mayordomo-Febrer A, López-Murcia M, Morales-Tatay JM, Monleón-Salvado D and Pinazo-Durán MD: Metabolomics of the aqueous humor in the rat glaucoma model induced by a series of intracameral sodium hyaluronate injection. *Exp Eye Res* 131: 84-92, 2015.
- Leruez S, Marill A, Bresson T, de Saint Martin G, Buisset A, Muller J, Tessier L, Gadras C, Verny C, Gohier P, *et al*: A metabolomics profiling of glaucoma points to mitochondrial dysfunction, senescence, and polyamines deficiency. *Invest Ophthalmol Vis Sci* 59: 4355-4361, 2018.
- Liu J, Cao C, Jin Y, Wang Y, Ma X, Li J, Guo S, Yang J, Niu J and Liang X: Induced neural stem cells suppressed neuroinflammation by inhibiting the microglial pyroptotic pathway in intracerebral hemorrhage rats. *iScience* 26: 107022, 2023.
- Kao YC, Ho PC, Tu YK, Jou IM and Tsai KJ: Lipids and Alzheimer's disease. *Int J Mol Sci* 21: 1505, 2020.
- Sastry PS: Lipids of nervous tissue: Composition and metabolism. *Prog Lipid Res* 24: 69-176, 1985.
- Smith JA, Nicaise AM, Ionescu RB, Hamel R, Peruzzotti-Jametti L and Pluchino S: Stem cell therapies for progressive multiple sclerosis. *Front Cell Dev Biol* 9: 696434, 2021.
- Kang EY, Liu PK, Wen YT, Quinn PMJ, Levi SR, Wang NK and Tsai RK: Role of oxidative stress in ocular diseases associated with retinal ganglion cells degeneration. *Antioxidants (Basel)* 10: 1948, 2021.
- Belforte N, Agostinone J, Alarcon-Martinez L, Villafranca-Baughman D, Dotigny F, Cueva Vargas JL and Di Polo A: AMPK hyperactivation promotes dendrite retraction, synaptic loss, and neuronal dysfunction in glaucoma. *Mol Neurodegener* 16: 43, 2021.
- Galan A, Dergham P, Escoll P, de-la-Hera A, D'Onofrio PM, Magharious MM, Koeberle PD, Frade JM and Saragovi HU: Neuronal injury external to the retina rapidly activates retinal glia, followed by elevation of markers for cell cycle re-entry and death in retinal ganglion cells. *PLoS One* 9: e101349, 2014.
- Syc-Mazurek SB, Fernandes KA and Libby RT: JUN is important for ocular hypertension-induced retinal ganglion cell degeneration. *Cell Death Dis* 8: e2945, 2017.
- Do JL, Allahwerdy S, David RC, Weinreb RN and Welsbie DS: Sheath-preserving optic nerve transection in rats to assess axon regeneration and interventions targeting the retinal ganglion cell axon. *J Vis Exp* 6: 3791/61748, 2020.
- Rosenberg LJ, Emery DG and Lucas JH: Effects of sodium and chloride on neuronal survival after neurite transection. *J Neuropathol Exp Neurol* 60: 33-48, 2001.

37. Gerdt J, Summers DW, Milbrandt J and DiAntonio A: Axon self-destruction: New links among SARM1, MAPKs, and NAD<sup>+</sup> metabolism. *Neuron* 89: 449-460, 2016.
38. Krishnan A, Kocab AJ, Zacks DN, Marshak-Rothstein A and Gregory-Ksander M: A small peptide antagonist of the Fas receptor inhibits neuroinflammation and prevents axon degeneration and retinal ganglion cell death in an inducible mouse model of glaucoma. *J Neuroinflammation* 16: 184, 2019.
39. Gertsman I and Barshop BA: Promises and pitfalls of untargeted metabolomics. *J Inher Metab Dis* 41: 355-366, 2018.
40. Di Minno A, Gelzo M, Stornaiuolo M, Ruoppolo M and Castaldo G: The evolving landscape of untargeted metabolomics. *Nutr Metab Cardiovasc Dis* 31: 1645-1652, 2021.
41. Hallett PJ, Engelender S and Isacson O: Lipid and immune abnormalities causing age-dependent neurodegeneration and Parkinson's disease. *J Neuroinflammation* 16: 153, 2019.
42. Bradke F, Fawcett JW and Spira ME: Assembly of a new growth cone after axotomy: The precursor to axon regeneration. *Nat Rev Neurosci* 13: 183-193, 2012.
43. Yang C, Wang X, Wang J, Wang X, Chen W, Lu N, Siniosoglou S, Yao Z and Liu K: Rewiring neuronal glycerolipid metabolism determines the extent of axon regeneration. *Neuron* 105: 276-292. e5, 2020.
44. Wang J, Wang Z, Zhang Y and Li J: Proteomic analysis of vitreal exosomes in patients with proliferative diabetic retinopathy. *Eye (Lond)* 37: 2061-2068, 2023.
45. Haines NR, Manoharan N, Olson JL, D'Alessandro A and Reisz JA: Metabolomics analysis of human vitreous in diabetic retinopathy and rhegmatogenous retinal detachment. *J Proteome Res* 17: 2421-2427, 2018.
46. Li L, Yang K, Li C, Zhang H, Yu H, Chen K, Yang X and Liu L: Metagenomic shotgun sequencing and metabolomic profiling identify specific human gut microbiota associated with diabetic retinopathy in patients with type 2 diabetes. *Front Immunol* 13: 943325, 2022.
47. Paris LP, Johnson CH, Aguilar E, Usui Y, Cho K, Hoang LT, Feitelberg D, Benton HP, Westenskow PD, Kurihara T, *et al*: Global metabolomics reveals metabolic dysregulation in ischemic retinopathy. *Metabolomics* 12: 15, 2016.
48. Ensari Delioğlu EN, Uğurlu N, Erdal E, Malekghasemi S and Çağır N: Evaluation of sphingolipid metabolism on diabetic retinopathy. *Indian J Ophthalmol* 69: 3376-3380, 2021.
49. Chaurasia RK, Singh R, Agrawal JK and Maurya OP: Sex hormones and diabetic retinopathy. *Ann Ophthalmol* 25: 227-230, 1993.
50. Aljohani AJ, Edwards G, Guerra Y, Dubovy S, Miller D, Lee RK and Bhattacharya SK: Human trabecular meshwork sphingolipid and ceramide profiles and potential latent fungal commensalism. *Invest Ophthalmol Vis Sci* 55: 3413-3422, 2014.
51. Kouassi Nzoughe J, Guehlouz K, Leruez S, Gohier P, Bocca C, Muller J, Blanchet O, Bonneau D, Simard G, Milea D, *et al*: A data mining metabolomics exploration of glaucoma. *Metabolites* 10: 49, 2020.
52. Qiu Y, Yu J, Tang L, Ren J, Shao M, Li S, Song Y, Cao W and Sun X: Association between sex hormones and visual field progression in women with primary open angle glaucoma: A cross-sectional and prospective cohort study. *Front Aging Neurosci* 13: 756186, 2021.
53. Chang R, Zhu Y, Xu J, Chen L, Su G, Kijlstra A and Yang P: Identification of urine metabolic biomarkers for Vogt-Koyanagi-Harada disease. *Front Cell Dev Biol* 9: 637489, 2021.
54. Warden C, Barnett JM and Brantley MA Jr: Taurocholic acid inhibits features of age-related macular degeneration in vitro. *Exp Eye Res* 193: 107974, 2020.
55. Sinha T, Ikelle L, Makia MS, Crane R, Zhao X, Kakakhel M, Al-Ubaiddi MR and Naash MI: Riboflavin deficiency leads to irreversible cellular changes in the RPE and disrupts retinal function through alterations in cellular metabolic homeostasis. *Redox Biol* 54: 102375, 2022.
56. Chen H, Chan AY, Stone DU and Mandal NA: Beyond the cherry-red spot: Ocular manifestations of sphingolipid-mediated neurodegenerative and inflammatory disorders. *Surv Ophthalmol* 59: 64-76, 2014.
57. Chiang JYL and Ferrell JM: Bile acid receptors FXR and TGR5 signaling in fatty liver diseases and therapy. *Am J Physiol Gastrointest Liver Physiol* 318: G554-G573, 2020.
58. MahmoudianDehkordi S, Arnold M, Nho K, Ahmad S, Jia W, Xie G, Louie G, Kueider-Paisley A, Moseley MA, Thompson JW, *et al*: Altered bile acid profile associates with cognitive impairment in Alzheimer's disease-An emerging role for gut microbiome. *Alzheimers Dement* 15: 76-92, 2019.
59. Rafiee Z, Garcia-Serrano AM and Duarte JMN: Taurine supplementation as a neuroprotective strategy upon brain dysfunction in metabolic syndrome and diabetes. *Nutrients* 14: 1292, 2022.
60. Bocca C, Le Pailh V, Chao de la Barca JM, Kouassy Nzoughe J, Amati-Bonneau P, Blanchet O, Védie B, Géromin D, Simard G, Procaccio V, *et al*: A plasma metabolomic signature of Leber hereditary optic neuropathy showing taurine and nicotinamide deficiencies. *Hum Mol Genet* 30: 21-29, 2021.
61. Seol SI, Kim HJ, Choi EB, Kang IS, Lee HK, Lee JK and Kim C: Taurine protects against postischemic brain injury via the antioxidant activity of taurine chloramine. *Antioxidants (Basel)* 10: 372, 2021.
62. Wu JY and Prentice H: Role of taurine in the central nervous system. *J Biomed Sci* 17 (Suppl 1): S1, 2010.
63. Menzie J, Prentice H and Wu JY: Neuroprotective mechanisms of taurine against ischemic stroke. *Brain Sci* 3: 877-907, 2013.
64. Jafri AJA, Agarwal R, Iezhitsa I, Agarwal P and Ismail NM: Taurine protects against NMDA-induced retinal damage by reducing retinal oxidative stress. *Amino Acids* 51: 641-646, 2019.
65. Wang X, Xie G, Zhao A, Zheng X, Huang F, Wang Y, Yao C, Jia W and Liu P: Serum bile acids are associated with pathological progression of hepatitis B-induced cirrhosis. *J Proteome Res* 15: 1126-1134, 2016.
66. Qi Y, Shi L, Duan G, Ma Y and Li P: Taurochenodeoxycholic acid increases cAMP content via specially interacting with bile acid receptor TGR5. *Molecules* 26: 7066, 2021.
67. Mahalak KK, Bobokalonov J, Firman J, Williams R, Evans B, Fanelli B, Soares JW, Kobori M and Liu L: Analysis of the ability of capsaicin to modulate the human gut microbiota in vitro. *Nutrients* 14: 1283, 2022.
68. Virseda-Berdices A, Rojo D, Martínez I, Berenguer J, González-García J, Brochado-Kith O, Fernández-Rodríguez A, Díez C, Hontañón V, Pérez-Latorre L, *et al*: Metabolomic changes after DAAs therapy are related to the improvement of cirrhosis and inflammation in HIV/HCV-coinfected patients. *Biomed Pharmacother* 147: 112623, 2022.
69. Abou-Ghali M and Stiban J: Regulation of ceramide channel formation and disassembly: Insights on the initiation of apoptosis. *Saudi J Biol Sci* 22: 760-772, 2015.
70. Alaamery M, Albeshri N, Aljawini N, Alsuwailm M, Massadeh S, Wheeler MA, Chao CC and Quintana FJ: Role of sphingolipid metabolism in neurodegeneration. *J Neurochem* 158: 25-35, 2021.
71. Petit CS, Lee JJ, Boland S, Swarup S, Christiano R, Lai ZW, Mejhert N, Elliott SD, McFall D, Haque S, *et al*: Inhibition of sphingolipid synthesis improves outcomes and survival in GARP mutant wobbler mice, a model of motor neuron degeneration. *Proc Natl Acad Sci USA* 117: 10565-10574, 2020.
72. Tham CS, Lin FF, Rao TS, Yu N and Webb M: Microglial activation state and lysophospholipid acid receptor expression. *Int J Dev Neurosci* 21: 431-443, 2003.
73. Scheiblich H, Schlütter A, Goldenbock DT, Latz E, Martínez-Martínez P and Heneka MT: Activation of the NLRP3 inflammasome in microglia: the role of ceramide. *J Neurochem* 143: 534-550, 2017.
74. Agudo-Barriuso M, Lahoz A, Nadal-Nicolás FM, Sobrado-Calvo P, Piquer-Gil M, Díaz-Llopis M, Vidal-Sanz M and Mullor JL: Metabolomic changes in the rat retina after optic nerve crush. *Invest Ophthalmol Vis Sci* 54: 4249-4259, 2013.
75. Woodcock J: Sphingosine and ceramide signalling in apoptosis. *IUBMB Life* 58: 462-466, 2006.
76. Burgess LG, Uppal K, Walker DI, Roberson RM, Tran V, Parks MB, Wade EA, May AT, Umfress AC, Jarrell KL, *et al*: Metabolome-wide association study of primary open angle glaucoma. *Invest Ophthalmol Vis Sci* 56: 5020-5028, 2015.
77. Schwedhelm E, Englisch C, Niemann L, Lezius S, von Lucadou M, Marmann K, Böger R, Peine S, Daum G, Gerloff C and Choe CU: Sphingosine-1-phosphate, motor severity, and progression in Parkinson's disease (MARK-PD). *Mov Disord* 36: 2178-2182, 2021.
78. Garcia CJ, Kosek V, Beltrán D, Tomás-Barberán FA and Hajslova J: Production of new microbially conjugated bile acids by human gut microbiota. *Biomolecules* 12: 687, 2022.
79. Styles NA, Shonsey EM, Falany JL, Guidry AL, Barnes S and Falany CN: Carboxy-terminal mutations of bile acid CoA:N-acyltransferase alter activity and substrate specificity. *J Lipid Res* 57: 1133-1143, 2016.



80. Reilly SJ, O'Shea EM, Andersson U, O'Byrne J, Alexson SE and Hunt MC: A peroxisomal acyltransferase in mouse identifies a novel pathway for taurine conjugation of fatty acids. *FASEB J* 21: 99-107, 2007.
81. Lin CL, Xu R, Yi JK, Li F, Chen J, Jones EC, Slutsky JB, Huang L, Rigas B, Cao J, *et al*: Alkaline ceramidase 1 protects mice from premature hair loss by maintaining the homeostasis of hair follicle stem cells. *Stem Cell Reports* 9: 1488-1500, 2017.
82. Hernández-Corbacho MJ, Salama MF, Canals D, Senkal CE and Obeid LM: Sphingolipids in mitochondria. *Biochim Biophys Acta Mol Cell Biol Lipids* 1862: 56-68, 2017.
83. Dalto DB, Tsoi S, Dyck MK and Matte JJ: Gene ontology analysis of expanded porcine blastocysts from gilts fed organic or inorganic selenium combined with pyridoxine. *BMC Genomics* 19: 836, 2018.



Copyright © 2023 Zhu et al. This work is licensed under a Creative Commons Attribution-NonCommercial-NoDerivatives 4.0 International (CC BY-NC-ND 4.0) License.